Radiation Physics and Chemistry 87 (2013) 46–52

Contents lists available at SciVerse ScienceDirect

Radiation Physics and Chemistry

journal homepage: www.elsevier.com/locate/radphyschem

# Location and size of nanoscale free-volume holes in crosslinked-polytetrafluoroethylene-based graft-type polymer electrolyte membranes determined by positron annihilation lifetime spectroscopy

Shin-ichi Sawada [a,*], Atsushi Yabuuchi [b], Masaki Maekawa [b], Atsuo Kawasuso [b], Yasunari Maekawa [a]

[a] Quantum Beam Science Directorate, Japan Atomic Energy Agency (JAEA) 1233 Watanuki, Takasaki, Gunma 370-1292, Japan
[b] Advanced Research Institute, Japan Atomic Energy Agency 1233 Watanuki, Takasaki, Gunma 370-1292, Japan

## HIGHLIGHTS

- Positron annihilation lifetime measurement of graft-type electrolyte membrane.
- There were two types of free-volume holes with different sizes.
- The smaller holes were located in the PTFE crystalline phases and grafted regions.
- The larger holes were located in the PTFE amorphous phases.

## ARTICLE INFO

*Article history:*
Received 19 September 2012
Accepted 12 February 2013
Available online 1 March 2013

*Keywords:*
Polymer electrolyte membrane
Gas permeation
Nanohole
Positron annihilation lifetime spectroscopy
Radiation grafting

## ABSTRACT

The location and size of nanoscale free-volume holes (nanoholes) in graft-type polymer electrolyte membranes (PEMs), which were prepared by radiation-induced graft polymerization (grafting) of styrene into crosslinked-polytetrafluoroethylene (cPTFE) films and subsequent sulfonation, were investigated using positron annihilation lifetime (PAL) spectroscopy. The PAL spectra of the PEMs indicated the existence of two types of *ortho*-positronium (*o*-Ps) species, corresponding to nanoholes with volumes of 0.11 and 0.38 $nm^3$. A comparison of the PAL data of the PEMs with that of the precursor original cPTFE and polystyrene-grafted films demonstrated the probability that the smaller holes were located in both the PTFE crystalline phases and the poly(styrene sulfonic acid) graft regions, whereas the larger holes are potentially localized in the PTFE amorphous phases. Taking into account both the size and the location of the nanoholes, it was concluded that gas transport through the larger holes in the amorphous PTFE phases was dominant over permeation through the smaller holes in the PTFE crystals and grafted regions.



## 1. Introduction

Polymer electrolyte membrane (PEM) fuel cells are electrochemical devices used to transform hydrogen and oxygen gases directly into electric power. In a PEM fuel cell, protons dissociated from hydrogen at the anode are conducted to the cathode through a PEM, where they react with oxygen to yield water. Recently, interest in PEM fuel cells has escalated owing to the high energy-conversion efficiency and low environmental load (Smitha et al., 2005; Dobrovol'skii et al., 2007). The most vital component in the fuel cell is the PEM, which acts as both an electrolyte for the conduction of protons and a separator to prevent mixing of the supplied fuel gases. At present, Nafion (DuPont Co.) is the most commonly used PEM for fuel cell applications because it exhibits the requisite properties such as good proton conductivity, mechanical strength, and chemical stability. Nafion consists of hydrophobic polytetrafluoroethylene (PTFE) backbones and pendant side chains of perfluorinated vinyl ethers binding sulfonic acid groups at the terminal (Mauritz and Moore, 2004).

One severe drawback of Nafion is the high permeability of the hydrogen and oxygen fuel gases through the membrane. That is, during the operation of a fuel cell employing Nafion, supplied hydrogen and oxygen gases permeate through the PEM to a certain extent (so-called gas crossover), resulting in fuel loss as well as a decline in the output cell voltage (Büchi et al., 1995a, 1995b; Wang, Capuano, 1998; Vie et al., 2002; Schmidt et al., 2005; Inaba et al., 2006). In addition, oxygen crossover from the cathode to the anode results in the serious problem of hydrogen peroxide generation. When oxygen reaches the anode, it reacts with protons to form hydrogen peroxide, which in turn leads to

* Corresponding author. Tel.: +81 27 346 9413; fax: +81 27 346 9687.
*E-mail address:* sawada.shinnichi@jaea.go.jp (S. Sawada).

0969-806X/$ - see front matter © 2013 Elsevier Ltd. All rights reserved.
http://dx.doi.org/10.1016/j.radphyschem.2013.02.016

oxidative degradation of the PEM (Inaba et al., 2006). Hence, suppression of gas permeation through PEMs is one promising strategy for improving the cell performance.

In general, gases and small molecules are believed to permeate through nanometer-size free-volume holes (nanoholes) in polymer films (Kobayashi et al., 1992; Haraya and Hwang, 1992; Tanaka et al., 1992; Fu et al., 2007). The structural features of nanoholes can be examined by means of positron annihilation lifetime (PAL) spectroscopy. This technique exploits the fact that the lifetime of *ortho*-positronium (*o*-Ps) (1–10 ns), which is longer than that of *para*-positronium (*p*-Ps) and free positron, is strongly correlated with hole size in solid materials such as polymers. To date, the majority of PAL studies regarding PEMs have focused on Nafion (Sodaye et al., 1997, 1998; Mohamed et al., 2008, 2009)

In the past decade, radiation-grafted PEMs have emerged as Nafion-alternative low-cost PEM materials (Nasef and Hegazy, 2004; Gubler et al., 2005). These graft-type PEMs are synthesized by three step processes involving pre-irradiation of fluoropolymer base films, grafting of styrene initiated from generated radicals, and sulfonation of aromatic rings of grafted polystyrene (PSt). The resultant PEMs possess fluoropolymer backbones and poly (styrene sulfonic acid) (PSSA) graft chains. With this method, the ion exchange capacity (IEC), *i.e.*, degree of grafting (DOG), can be controlled in the wide range of 0.5–3.0 meq/g by varying the experimental conditions such as pre-irradiation dose and grafting time. This advantage is not present in Nafion, whose IEC is fixed at about 0.90 meq/g. In our recent researches on the graft-type PEMs, it was revealed that the IEC of the PEMs was crucial factor influencing their morphology (Sawada et al., 2010a) and transport properties such as proton conductivity (Sawada and Maekawa, 2011) and water permeability (Sawada et al., 2008). Then, it became one of our main concerns to examine the nanohole structures of the graft-type PEMs with various ionic contents.

Quite recently, we have performed the PAL measurement of the graft-type PEMs based on crosslinked-polytetrafluoroethylene (cPTFE) to determine both the location and size of nanoholes in the PEMs. The hole size in the cPTFE PEMs is easily estimated from the *o*-Ps lifetime data. However, it is difficult to specify the exact location of nanoholes solely on the basis of PAL spectroscopy of the PEMs. Thus, as reference materials, the precursor original cPTFE and PSt-grafted films were also subjected to PAL measurements. It was anticipated that the three most probable locations of the nanoholes may be PTFE crystalline and amorphous phases, and grafted regions, derived from the parent precursor cPTFE and PSt-grafted films. Specifically, a comparison of the PAL data of the PEMs with those of the cPTFE and grafted films should provide meaningful information on the nanohole locations. Up to now, we reported the preliminary results of the PAL measurements in the conference proceedings (Sawada et al., 2009, 2010b). In this paper, the nanohole structures of the cPTFE film, PSt-grafted films, and PEMs are discussed in detail and clearly, and additionally, the gas transport behavior through the nanoholes in the PEMs is examined.

## 2. Experimental

### 2.1. Synthesis of PEMs

The graft-type PEMs were prepared as previously reported (Yamaki et al., 2004). A 42-μm-thick cPTFE film crosslinked in the molten state at about 340 °C using 100-kGy electron beam irradiation was used as a base material. The cPTFE film was pre-irradiated with a 15-kGy γ-ray in an Ar atmosphere at room temperature, and then immersed in a styrene monomer at 60 °C for 2–18 h. After graft polymerization, the film was immersed in toluene to extract any excess styrene monomers. The grafted film was then dried under vacuum at 40 °C to a constant weight. The DOG was estimated using the following equation:

$$\mathrm{DOG} = \frac{W_G - W_O}{W_O} \times 100, \quad (1)$$

where $W_O$ and $W_G$ denote the weights of the base cPTFE and grafted films, respectively.

For sulfonation, the grafted film was immersed in a 0.2 M mixture of chlorosulfonic acid and 1,2-dichloroethane at 50 °C for 6 h. Finally, the obtained PEM was rinsed with purified water and then dried in a vacuum oven. Fig. 1 shows the structural formulae of the base cPTFE film, PSt-grafted film, and PEM.

### 2.2. PAL measurement

PAL measurements were carried out using a conventional "fast–fast" coincidence system with a time resolution of 225 ps. A $^{22}$Na positron source was prepared by depositing and drying an aqueous solution of $^{22}$NaCl on a titanium thin film. This substrate (1 cm × 1 cm) was covered with another titanium film of the same size. The edges of the two titanium films were glued together in order to completely seal the radioactive $^{22}$NaCl. A stack of about 10 PEM samples was set on each side of the titanium films containing the positron source ($^{22}$NaCl) to ensure positron annihilation only in the samples. All of the PAL measurements were conducted at room temperature. The obtained PAL spectra with about $10^6$ counts were analyzed using the PATFIT program (Kirkegaard et al., 1981). As references, PAL spectra of the original cPTFE and PSt-grafted films were measured in the same way. In the PATFIT program, the accuracy of the fitting is expressed by the so-called variance of the fit (VOF), which is a normalized sum of the squares of the deviations between the fitted curve and the measured spectrum. As the fitting accuracy is higher, the VOF value is close to unity.

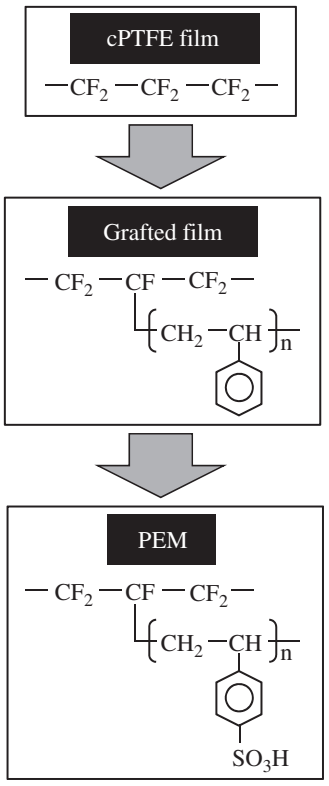


**Fig. 1.** Structural formulae of the cPTFE film, PSt-grafted film, and PEM.

## 3. Results and discussion

### 3.1. cPTFE base film

The positron annihilation count at time $t$, $C(t)$, is a sum of certain exponential terms corresponding to various lifetime components, and it is expressed by the following equation:

$$C(t) = \sum_{i=1}^{m} \frac{A_i}{\tau_i} \exp\left(-\frac{t}{\tau_i}\right), \tag{2}$$

where $\tau_i$ and $A_i$ denote the lifetime and intensity of component $i$, respectively. Relative intensity of component $i$, $I_i$, is estimated as follows:

$$I_i = \frac{A_i}{\sum_{i=1}^{m} A_i}. \tag{3}$$

The $\tau_i$ and $I_i$ of all the lifetime components were optimized by least-square fitting of the experimentally-obtained $C(t)-t$ curves to Eq. (2). In general, the PAL spectra are deconvoluted into three terms corresponding to $p$-Ps, free positron, and $o$-Ps. In previous PAL studies on Nafion (Sodaye et al., 1997, 1998; Mohamed et al., 2008, 2009), the three-term analysis was performed to extract the lifetime and relative intensity of $o$-Ps, thus providing insight into the nature of the nanoholes.

Fig. 2 shows the PAL spectrum of the cPTFE film. In this case, it was not possible to execute a three-term analysis by PATFIT program to determine the values of $\tau_i$ and $I_i$. On the contrary, a four-term analysis was successfully completed with the VOF of 1.02, indicating sufficient fitting accuracy. The obtained four components 1–4, having unique $\tau_i$ and $I_i$ ($i=1-4$), were tentatively ascribed to $p$-Ps, free positron, and two kinds of $o$-Ps based on the order of the lifetime from the shortest to the longest ($\tau_1=0.18$ ns, $\tau_2=0.42\pm0.01$ ns, $\tau_3=2.29\pm0.19$ ns, $\tau_4=4.47\pm0.12$ ns, $I_1=35.1\pm1.4\%$, $I_2=37.5\pm1.2\%$, $I_3=9.8\pm1.4\%$, $I_4=17.6\pm1.6\%$). The position, at which the annihilation of each of the two-types of $o$-Ps takes place, is addressed in the ensuing paragraph.

A previous PAL study on non-crosslinked PTFE films (Mohamed et al., 2007) reported a similar observation of two $o$-Ps with shorter and longer lifetimes attributed to the annihilation in the crystalline and amorphous phases of PTFE. In the crystalline phases, the polymer chains are regularly and densely packed with small intermolecular free-volume voids. In contrast, in the amorphous phases, the polymer chain configuration is random, thereby forming larger free-volume spaces between polymer chains. In view of these facts, it was assumed that the shorter-lived $o$-Ps ($\tau_3=1.1$ ns) and longer-lived $o$-Ps ($\tau_4=3.9$ ns) existed in the PTFE crystalline and amorphous phases, respectively. The base cPTFE used in the current study is also a crystalline polymer that exhibits a crystallinity of ca. 33% as estimated from differential scanning calorimetry (Chen et al., 2006). On this basis, it was deduced that components 3 ($\tau_3=2.29$ ns) and 4 ($\tau_4=4.47$ ns) for the cPTFE film were $o$-Ps in the crystalline and amorphous phases, respectively.

Notably, both $\tau_3$ ($=2.29$ ns) and $\tau_4$ ($=4.47$ ns) for the cPTFE film were longer than those for the non-crosslinked PTFE film ($\tau_3=1.1$ ns, $\tau_4=3.9$ ns), suggesting that the PTFE molecular conformation was altered by crosslinkings. In the amorphous phases, it is expected that the crosslinking points prevented tight entanglement of the PTFE polymer chains, resulting in making the intermolecular voids larger. This was likely the reason for a longer $\tau_4$ for the cPTFE relative to that of non-crosslinked PTFE. Furthermore, crosslinking of polymers is considered to deteriorate the alignment of the polymer chains around the crystallites (Oshima et al., 1997). Accordingly, strictly speaking, component 3 for the cPTFE film may be attributed to the $o$-Ps not only in the PTFE crystals but also in the disordered boundary regions between the crystalline and amorphous phases, where the interstitial spaces between the polymer chains are slightly larger than those in the normal crystals. Consequently, $\tau_3$ for the cPTFE film was longer than that for the non-crosslinked film.

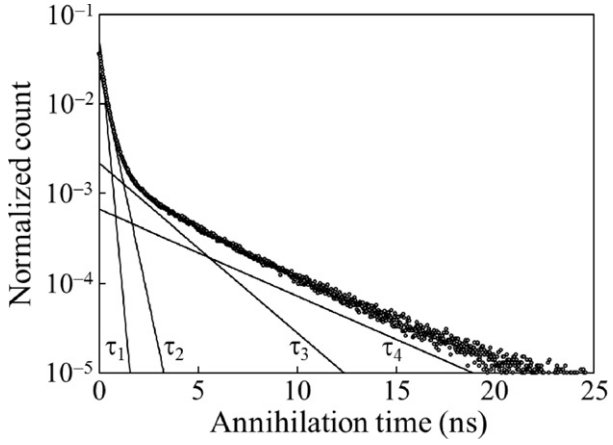


**Fig. 2.** PAL spectrum of the cPTFE film. The straight lines corresponding to the $\tau_i$ ($i=1$–4) were also depicted in this figure.

### 3.2. Grafted films

Prior to the discussion of the PAL measurement results for the grafted films, an understanding of the radiation grafting process onto base polymer films is necessary. Ionizing radiations such as $\gamma$-rays and electron beams homogeneously produce free radicals in base polymer films. The radicals in the amorphous phases quickly vanish through recombination and disproportionation reactions of two radicals, whereas those in the crystalline phases where polymer chain motion is strongly restricted can survive for days and weeks. When the radicals in the crystalline phases migrate to the crystalline/amorphous boundaries, they encounter monomers that can diffuse only in the amorphous phases, leading to the initiation of graft polymerization. This grafting kinetics was experimentally confirmed by an electron spin resonance method (Seguchi and Tamura, 1973, 1974), an X-ray diffraction method (Smit and Bezjak, 1981) and a time-resolved small-angle neutron scattering (SANS) method (Iwase et al., 2011). In the case of styrene grafting into fluoropolymer base films, it was found from SANS measurements that the PSt graft chains were elongated into amorphous phases and formed the PSt-grafted regions phase-separated from fluoropolymer domains (Iwase et al., 2011).

Like the cPTFE film, the PAL spectra of all of the PSt-grafted films were deconvoluted into four components with the VOF range of 0.97–1.13. Fig. 3 shows the $\tau_i$ and $I_i$ ($i=3,4$) values of the two types of $o$-Ps in the PSt-grafted films as a function of DOG. A remarkable increase in $I_3$ was observed with increasing DOG (see Fig. 3(A)), indicating the expansion of the region available for formation of the shorter-lived $o$-Ps with increasing DOG. However, it is well known that the crystallinity does not increase, and may even decrease, because of styrene grafting into PTFE films (Nasef, 2002). Thus, one possible explanation for the $I_3$–DOG relationship is that component 3 involves $o$-Ps species in both the PTFE crystalline phases and the PSt-grafted regions. In fact, the $o$-Ps lifetime in PSt (1.94 ns (Honda et al., 2007)) and PTFE crystallites (2.29 ns) seemed too similar to be differentiated from each other in PAL spectra analysis. The assignment of component 3 is further supported by the fact that $\tau_3$ appeared to be the weight-averaged $o$-Ps lifetime in both the PTFE crystalline phases and grafted regions. That is, $\tau_3$ decreased slightly with increasing

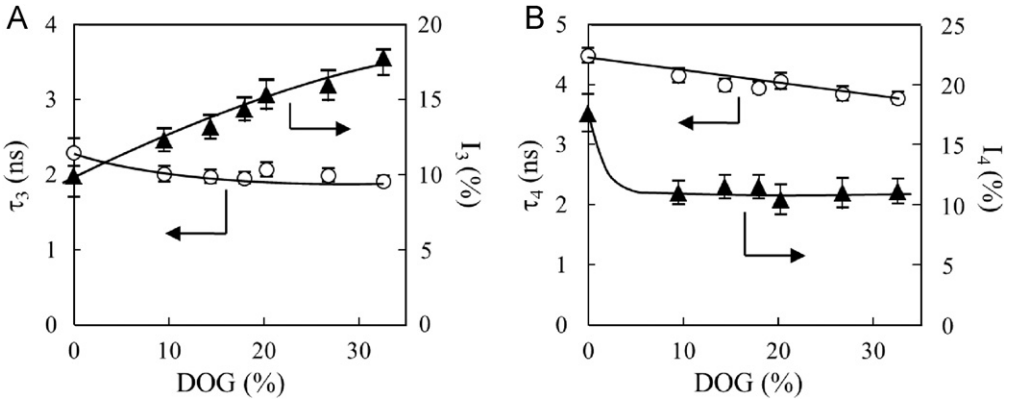


**Fig. 3.** Lifetimes ($\tau_3$ and $\tau_4$) and relative intensities ($I_3$ and $I_4$) of *o*-Ps in PSt-grafted films as functions of DOG. The curves depicted in these figures were eye guides.

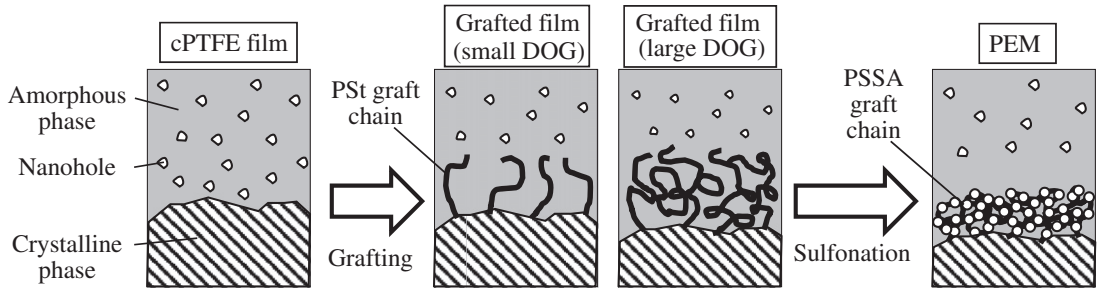


**Fig. 4.** Schematic images of the nanoholes in the PTFE amorphous phases. The nanoholes near the crystalline phases were extinguished at small DOG, while the remained nanoholes were shrinked at large DOG. The nanohole size of the PEMs reverted to the same level as that of the base cPTFE film.

DOG (see Fig. 3(A)), because the relative ratio of the shorter-lived *o*-Ps in the grafted regions to the longer-lived *o*-Ps in the cPTFE crystalline phases became higher with increasing DOG.

In the case of component 4, $I_4$ decreased significantly when the grafted PSt was introduced into cPTFE even in low DOG ranges ($<10\%$), and subsequently reached a plateau value at higher DOG. On the other hand, $\tau_4$ exhibited a gradual decline with increasing DOG (see Fig. 3(B)). Trends similar to those of the *o*-Ps lifetime and relative intensity were observed in a PAL study of the other PSt-grafted films based on poly(tetrafluoroethylene-*co*-hexafluoropropylene) (Sudarshan et al., 2007). In the current case, the behavior of $\tau_4$ and $I_4$ upon grafting can be explained by taking into account the radiation grafting process. As mentioned above, the grafting reaction is initiated by polymer radicals generated by pre-irradiation in the PTFE crystalline/amorphous boundary. At DOG values below 10%, it is likely that the PSt graft chains are propagated into the PTFE amorphous phases to directly occupy and extinguish the nanoholes. Hence, the number of nanoholes declined rapidly as reflected in the sharp drop in $I_4$. At DOG values above 10%, graft chain propagation should preferentially occur in the pre-grafted PSt regions rather than in the amorphous PTFE phases; thus, the number of nanoholes was presumed to be constant. It is expected that the expansion of the grafted regions induced certain stress and compression of the amorphous PTFE phases throughout the films. This probably causes shrinkage of the interstitial voids, leading to a gradual decrease of $\tau_4$ with increasing DOG. A schematic representation of the nanoholes in the PTFE amorphous phases is shown in Fig. 4. This figure depicts the extinction of nanoholes near the PTFE crystalline phases at small DOG and shrinkage of remaining nanoholes at large DOG.

### 3.3. PEMs

The PAL measurements were performed on the two PEMs with IEC of 1.1 and 1.8 meq/g, which corresponds to the DOGs of 14% and 27%, respectively. The PAL spectra of these PEMs were also deconvoluted into four lifetime components with the VOF range of 0.98–1.06. In line with the above argument, components 3 and 4 were assigned as the sum of the *o*-Ps in the PTFE crystalline phases/PSSA graft regions and the PTFE amorphous phases. Fig. 5 shows the $\tau_i$ ($i=3,4$) values of the cPTFE film, PSt-grafted films, and PEMs with DOGs of 14% and 27%. For both DOG, $\tau_3$ of the PEMs (2.13–2.14 ns) was similar to that of the PSt-grafted films (1.96–1.99 ns), suggesting no significant change in the nanohole structures in the PTFE crystalline phases and grafted regions of the PEMs relative to the grafted films.

On the other hand, $\tau_4$, which was assigned to the *o*-Ps lifetime in the PTFE amorphous phases, was longer for the PEMs of both DOGs (4.38–4.55 ns) than that for the PSt-grafted films (3.84–3.99 ns), and even seemed to revert to the $\tau_4$ value of the original cPTFE film (4.47 ns) (see Fig. 5). This result can be explained by considering the following structural change. As mentioned above, the PSt graft chains would be somewhat entangled with PTFE chains, and would directly occupy or indirectly compress the nanoholes in the amorphous phases. In contrast to such relative miscibility between the PSt graft and PTFE chains, the PSSA graft and PTFE chains in the PEMs were probably fully immiscible to each other, because the former and latter chains are hydrophilic and hydrophobic, respectively. For this reason, it is anticipated that the amorphous PTFE phases excluded the PSSA graft chains owing to the strong repulsive interactions (*i.e.*, phase separation). Thus, the nanoholes in the PTFE amorphous phases should recover to the original level in the cPTFE film as shown in Fig. 4.

Fig. 6 shows the $I_i$ ($i=3,4$) for the cPTFE film, grafted films, and PEMs with DOGs of 14% and 27%. For both the DOGs, $I_3$ and $I_4$ of the PEMs declined significantly relative to the grafted films. Similar results were reported in the PAL study of poly(ether ether ketone) (PEEK) films before and after sulfonation (Kobayashi et al., 2009). In the referenced report, the *o*-Ps yield for sulfonated PEEK (sPEEK) was far lower than that of the non-sulfonated PEEK.

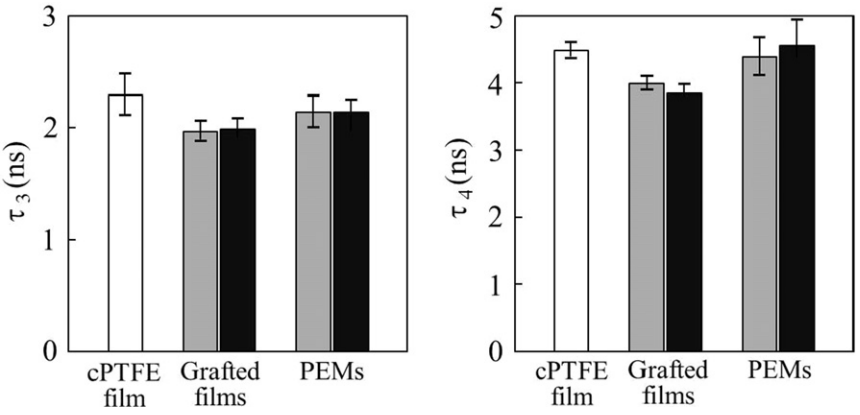


**Fig. 5.** Lifetimes ((left) $\tau_3$ and (right) $\tau_4$) for the cPTFE film, PSt-grafted films, and PEMs with DOGs of (gray) 14% and (black) 27%.

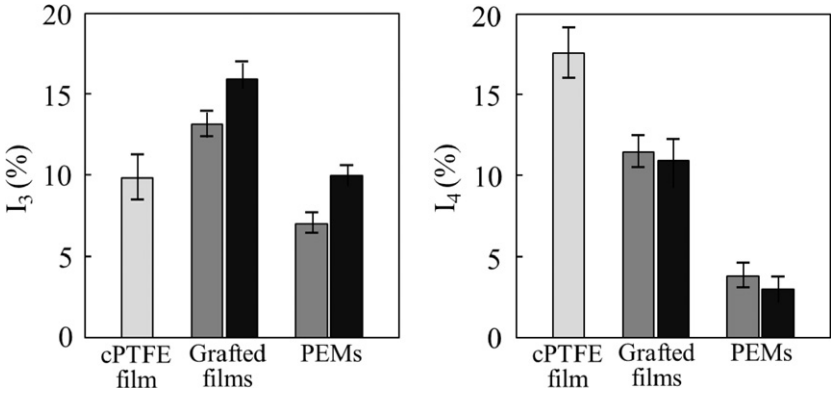


**Fig. 6.** Relative intensities ((left) $I_3$ and (right) $I_4$) for the cPTFE film, PSt-grafted films, and PEMs with DOGs of (gray) 14% and (black) 27%.

This phenomenon was termed "inhibition of Ps formation", and was presumed to occur as follows (Kobayashi et al., 2009). Since the sulfonic acid group is an electron withdrawing component, the sulfonic-acid-substituted aromatic ring becomes electron deficient and electron acceptor. Some of the spur electrons tend to be captured by the electron acceptors (sulfonated aromatic rings), and hence cannot recombine with positrons to form Ps. Accordingly, there were not sufficient available electrons to react, thereby suppressing the formation of Ps. It is to be recalled here that the cPTFE PEMs also possess sulfonated aromatic rings in the PSSA graft chains. Therefore, the Ps-formation inhibition process would take place, resulting in a decrease of both $I_3$ and $I_4$.

The next point of interest is the size of the nanoholes, which is strongly correlated with the *o*-Ps lifetime. There are many equations relating the *o*-Ps lifetime to the void size by assuming various shapes of nanoholes such as a sphere, cubic, cuboid, layer, and cylindrical channel (Consolati, 2002). Since we had no information about nanohole shape, we assumed that the nanoholes in the cPTFE PEMs were spherical. This assumption of the spherical nanoholes has been widely adopted in many previous PAL measurements on polymer materials. The semi-empirical relationship between the *o*-Ps lifetime, $\tau_i$ (ns), and the radius of the spherical nanoholes, $R_i$ (nm), is expressed by the Tao–Eldrup equation (Tao, 1972; Eldrup et al., 1981):

$$\tau_i = \frac{1}{2}\left[1-\frac{R_i}{R_i+\Delta R}+\frac{1}{2\pi}\sin\left(\frac{2\pi R_i}{R_i+\Delta R}\right)\right]^{-1} \quad (i=3,4), \tag{4}$$

where $\Delta R$ denotes a fitted empirical electron-layer thickness ($=0.166$ nm). The $R_i$ was calculated by substituting $\tau_i$ into Eq. (4). The nanohole volume, $V_i$, was also calculated according to the relationship:

$$V_i = \frac{4}{3}\pi R_i^3 \quad (i=3,4). \tag{5}$$

**Table 1**
Results of PAL measurements of graft-type PEMs.

| DOG (%) | 14 | | 27 | |
|---|---|---|---|---|
| Component *i* | 3 | 4 | 3 | 4 |
| $\tau_i$ (ns) | $2.14\pm0.14$ | $4.38\pm0.29$ | $2.14\pm0.10$ | $4.55\pm0.38$ |
| $I_i$ (%) | $7.1\pm0.6$ | $3.8\pm0.8$ | $10\pm0.6$ | $3.0\pm0.7$ |
| $R_i$ (nm) | $0.30\pm0.01$ | $0.44\pm0.02$ | $0.30\pm0.01$ | $0.45\pm0.02$ |
| $V_i$ (nm$^3$) | $0.11\pm0.01$ | $0.37\pm0.03$ | $0.11\pm0.01$ | $0.39\pm0.04$ |

Table 1 shows the determined $\tau_i$, $I_i$, $R_i$ and $V_i$ ($i=3,4$) values. The $V_3$ was 0.11 nm$^3$ for the PEMs of both DOGs, whereas the $V_4$ was 0.37 and 0.39 nm$^3$ for the respective DOGs values of 14% and 27%. From the above discussion, the smaller holes ($V_3$) should be present in the PTFE crystallites as well as the PSSA grafts, whereas the larger holes ($V_4$) are likely to be localized in the amorphous PTFE phases. In previous PAL spectroscopy studies on Nafion, the size of the nanoholes was estimated, but the location of these holes was not precisely identified (Sodaye et al., 1997, 1998). Herein, direct comparison of the PAL data of the graft-type PEMs with the precursor original cPTFE and PSt-grafted films enabled us to comprehend not only the size of the nanoholes but also their locations.

According to the classical free-volume theory, the segmental motion of polymers is considered to incessantly generate and dissipate free-volume nanoholes. The penetrant molecules in

polymers can diffuse when they find neighboring holes large enough to move. The self-diffusion coefficient of penetrant molecules, $D$, is expressed as follows (Cohen and Turnbull, 1959; Fujita, 1961):

$$D = K_1 R\,T \exp\left(-\frac{K_2}{r_V}\right), \quad (6)$$

where $K_1$ depends on the size and shape of the diffusion molecule, and $K_2$ is related to the minimal size of nanoholes through which diffusional jumping of penetrants occurs. The other parameters, $R$, $T$, and $r_V$ denote the gas constant, absolute temperature, and volumetric ratio of the nanoholes to total polymer matrices, respectively.

In recent years, it has been recognized that D of penetrants in polymers is affected by not only $r_V$ but also other parameters (Tanaka et al., 1992, 2000). Tanaka et al. (2000) revealed that $D$ in some polyimides strongly depended on the individual nanohole size, $V$, measured by PAL spectroscopy. They proposed the following empirical relationship between $D$ and $V$:

$$D = A\,R\,T \exp\left(-\frac{B}{V}\right), \quad (7)$$

where $A$ and $B$ denote the constants related to the types of gases and polymers. Furthermore, Tanaka et al. (2000) also found that polymers with higher glass transition temperature ($T_g$) exhibited lower $D$ compared to those with low $T_g$. This observation is presumably attributed to the inactive molecular motion in the high-$T_g$ polymers. Their stiff polymer chains would restrict the generation and dissipation of intermolecular free-volume holes, thereby retarding penetrant diffusion. Therefore, the gas diffusion in polymers is assumed to be influenced by two main factors: the size of individual nanoholes; the mobility of polymer chains surrounding the nanoholes.

Finally, based on the results of the PAL measurements at room temperature, we present a discussion of the gas transport through nanoholes in the cPTFE-based graft-type PEMs. Recall that the nanohole size in the PTFE amorphous phases was three-times larger than that in the PTFE crystalline phases and PSSA-grafted regions (see Table 1). Since $D$ is an exponential function of $V$ as shown in Eq. (7), the hole size of the polymers should affect the $D$ value significantly. Thus, from the viewpoint of $V$, gas molecules are predicted to pass primarily through the larger nanoholes present in the PTFE amorphous phases.

Let us now take into account another determining factor of $D$, *i.e.*, polymer chain mobility. The PTFE amorphous phases containing the larger holes had $T_g$ values ranging from $-60$ °C to $-35$ °C (Ohzawa and Wada, 1964), which are far lower than room temperature. Thus, the amorphous PTFE chains should possess sufficient thermal mobility to drive gas diffusion. This situation is probably quite the opposite for the smaller holes located in both the PTFE crystalline phases and the PSSA grafted regions. The PTFE chains in the crystalline phases are almost immobilized at room temperature, since their melting point is 340 °C (Ohzawa and Wada, 1964). The PSSA chains also have less motional freedom because the $T_g$ of PS (backbones of PSSA graft chains) is 107 °C (Rieger, 1996). These facts suggest that the molecular motion of polymer chains surrounding the smaller nanoholes should be restricted, thus impeding gas diffusion. Consequently, it follows from the above arguments that gas permeation through the larger nanoholes is dominant over permeation through the smaller holes.

Because the constants $A$ and $B$ in Eq. (7) are unknown, quantitative evaluation of $D$ is not possible in this study. In the near future, we will conduct hydrogen and oxygen permeation experiments for the graft-type PEMs to determine their gas permeability, and to examine the gas transport mechanism related to the nanohole structures using PAL spectroscopy as a probe technique.

## 4. Conclusion

The location and size of nanoholes in cPTFE-based graft-type PEMs was investigated by PAL spectroscopy. In order to gain deeper insight into the nature of the nanoholes, PAL measurements were also performed for the precursor base cPTFE and PSt-grafted films. Analysis of the PAL spectra of all the samples yielded the two types of *o*-Ps with different lifetimes. From the *o*-Ps lifetime ($\tau_3$ and $\tau_4$), the size of the nanoholes in the PEMs was calculated to be 0.11 and 0.38 $nm^3$, respectively. Comparison of the PAL spectra of the PEMs with those of cPTFE and grafted films allowed elucidation of the location of nanoholes. In the PEMs, the smaller holes were deduced to be located in both the PTFE crystalline phases and the PSSA grafted regions, while the larger holes were plausibly located in the PTFE amorphous phases. Finally, the gas transport behavior in the PEMs was examined from the viewpoints of the size of individual nanoholes and the mobility of polymer chains surrounding the nanoholes. The nanohole size in the PTFE amorphous phases was more than three-times larger than that in the PTFE crystalline phases and PSSA-grafted regions. In addition, the amorphous PTFE chains were assumed to undergo reasonable molecular motion. Accordingly, it was concluded that gas transport through the larger nanoholes in the PTFE amorphous phases would be dominant over permeation through the smaller holes in the PTFE crystals and PSSA-grafted regions.

## References


Büchi, F.N., Gupta, B., Haas, O., Scherer, G.G., 1995a. Performance of differently cross-linked, partially fluorinated proton exchange membranes in polymer electrolyte fuel cells. J. Electrochem. Soc. 142, 3044–3048.

Büchi, F.N., Gupta, B., Haas, O., Scherer, G.G., 1995b. Study of radiation-grafted FEP-g-polystyrene membranes as polymer electrolytes in fuel cells. Electrochim. Acta. 40, 345–353.

Chen, J., Asano, M., Maekawa, Y., Yoshida, M., 2006. Suitability of some fluoropolymers used as base films for preparation of polymer electrolyte fuel cell membranes. J. Membr. Sci. 277, 249–257.

Cohen, M.H., Turnbull, D., 1959. Molecular transport in liquids and glasses. J. Chem. Phys. 31, 1164–1169.

Consolati, G., 2002. Positronium trapping in small voids: influence of their shape on positron annihilation results. J. Chem. Phys. 117, 7279–7283.

Dobrovol'skii, Y.A., Volkov, E.V., Pisareva, A.V., Fedotov, Y.A., Likhachev, D.Y., Rusanov, A.L., 2007. Proton-exchange membranes for hydrogen–air fuel cells. Russ. J. Gen. Chem. 77, 766–777.

Eldrup, M., Lightbody, D., Sherwood, J.N., 1981. The temperature dependence of positron lifetimes in solid pivalic acid. Chem. Phys. 63, 51–58.

Fu, Y.J., Hu, C.C., Lee, K.R., Tsai, H.A., Ruaan, R.C., 2007. The correlation between free volume and gas separation properties in high molecular weight poly(methyl methacrylate) membranes. Eur. Polym. J. 43, 959–967.

Fujita, H., 1961. Diffusion in polymer-diluent systems. Fortschr. Hochpolym. Forsch. 3, 1–47.

Gubler, L., Gürsel, S.A., Scherer, G.G., 2005. Radiation grafted membranes for polymer electrolyte fuel cells. Fuel Cells 5, 317–335.

Haraya, K., Hwang, S.T., 1992. Permeation of oxygen, argon and nitrogen through polymer membranes. J. Membr. Sci. 71, 13–27.

Honda, Y., Shimada, T., Tashiro, M., Kimura, N., Yoshida, Y., Isoyama, G., Tagawa, S., 2007. Study of annihilation processes of positrons in polystyrene-related polymers. Radiat. Phys. Chem. 76, 169–171.

Inaba, M., Kinumoto, T., Kiriake, M., Umebayashi, R., Tasaka, A., Ogumi, Z., 2006. Gas crossover and membrane degradation in polymer electrolyte fuel cells. Electrochim. Acta 51, 5746–5753.

Iwase, H., Sawada, S., Yamaki, T., Maekawa, Y., Koizumi, S., 2011. Preirradiation graft polymerization of styrene in a poly(tetrafluoroethylene) film investigated by time-resolved small-angle neutron scattering. Int. J. Polym. Sci., Article ID 301807, 7 pp.

Kirkegaard, P., Eldrup, M., Mogensen, O.E., Pedersen, N.J., 1981. Program system for analysing positron lifetime spectra and angular correlation curves. Comp. Phys. Commun. 23, 307–335.

Kobayashi, Y., Haraya, K., Kamiya, Y., Hattori, S., 1992. Correlation between the *ortho*-positronium pick-off annihilation lifetime and the free volume in molecular liquids and polymers. Bull. Chem. Soc. Jpn. 65, 160–163.

Kobayashi, Y., Mohamed, H.F.M., Ohira, A., 2009. Positronium formation in aromatic polymer electrolytes for fuel cells. J. Phys. Chem. B 113, 5698–5701.
Mauritz, K.A., Moore, R.B., 2004. State of understanding of nafion. Chem. Rev. 104, 4535–4585.
Mohamed, H.F.M., Hady, E.E.A., Mohamed, S.S., 2007. Temperature dependence of the free volume in polytetrafluoroethylene studied by positron annihilation spectroscopy. Radiat. Phys. Chem. 76, 160–164.
Mohamed, H.F.M., Ito, K., Kobayashi, Y., Takimoto, N., Takeoka, Y., Ohira, A., 2008. Free volume and permeabilities of $O_2$ and $H_2$ in Nafion membranes for polymer electrolyte fuel cells. Polymer 49, 3091–3097.
Mohamed, H.F.M., Kobayashi, Y., Kuroda, C.S., Ohira, A., 2009. Effects of ion exchange on the free volume and oxygen permeation in Nafion for fuel cells. J. Phys. Chem. B 113, 2247–2252.
Nasef, M.M., 2002. Structural investigation of polystyrene grafted and sulfonated poly(tetrafluoroethylene) membranes. Eur. Polym. J. 38, 87–95.
Nasef, M.M., Hegazy, E.S.A., 2004. Preparation and applications of ion exchange membranes by radiation-induced graft copolymerization of polar monomers onto non-polar films. Prog. Polym. Sci. 29, 499–561.
Ohzawa, Y., Wada, Y., 1964. Mechanical relaxations and transitions in polytetrafluoroethylene. Jpn. J. Appl. Phys. 3, 436–447.
Oshima, A., Ikeda, S., Seguchi, T., Tabata, Y., 1997. Improvement of radiation resistance for polytetrafluoroethylene (PTFE) by radiation crosslinking. Radiat. Phys. Chem. 49, 279–284.
Rieger, J., 1996. The glass transition temperature of polystyrene. J. Therm. Anal. 46, 965–972.
Schmidt, T.J., Simbeck, K., Scherer, G.G., 2005. Influence of Cross-linking on performance of radiation-grafted and sulfonated FEP 25 MEmbranes in $H_2$–$O_2$ PEFC. J. Electrochem. Soc. 152, A93–A97.
Sawada, S., Yamaki, T., Nishimura, H., Asano, M., Suzuki, A., Terai, T., Maekawa, Y., 2008. Water transport properties of crosslinked-PTFE based electrolyte membranes. Solid State Ionics 179, 1611–1614.
Sawada, S., Kawasuso, A., Maekawa, M., Suzuki, A., Terai, T., Maekawa, Y., 2009. Positron annihilation lifetime study of graft-type fluorinated polymer electrolyte membranes. Mater. Sci. Forum 607, 70–72.
Sawada, S., Yamaki, T., Ozawa, T., Suzuki, A., Terai, T., Maekawa, Y., 2010a. Structural analysis of radiation-grafted polymer electrolyte membranes by dissipative particle dynamics simulation. Kobunshi Ronbunshu 67, 224–227, in Japanese.
Sawada, S., Kawasuso, A., Maekawa, M., Yabuuchi, A., Maekawa, Y., 2010b. Free-volume structure of fluoropolymer-based radiation-grafted electrolyte membranes investigated by positron annihilation lifetime spectroscopy. J. Phys. Conf. Ser. 225, 012048.
Sawada, S., Maekawa, Y., 2011. Proton conduction characteristics in radiation-grafted polymer electrolyte membranes based on perfluorinated and aromatic hydrocarbon polymers. ECS Trans. 41, 2125–2133.
Seguchi, T., Tamura, N., 1973. Mechanism of decay of alkyl radicals in irradiated polyethylene on exposure to air as studied by electron spin resonance. J. Phys. Chem. 77, 40–44.
Seguchi, T., Tamura, N., 1974. Electron spin resonance studies on radiation graft copolymerization in polyethylene II. Grafting initiated by allyl radicals trapped in irradiated polyethylene. J. Polym. Sci. Polym. Chem. Ed. 12, 1953–1964.
Smit, I., Bezjak, A., 1981. Structural changes in the grafted copolymer polyethylene–styrene. Polymer 22, 590–596.
Smitha, B., Sridhar, S., Khan, A.A., 2005. Solid polymer electrolyte membranes for fuel cell applications—a review. J. Membr. Sci. 259, 10–26.
Sodaye, H.S., Pujari, P.K., Goswami, A., Manohar, S.B., 1997. Probing the microstructure of Nafion-117 using positron annihilation spectroscopy. J. Polym. Sci. B: Polym. Phys. 35, 771–776.
Sodaye, H.S., Pujari, P.K., Goswami, A., Manohar, S.B., 1998. Measurement of free-volume hole size distribution in Nafion-117 using positron annihilation spectroscopy. J. Polym. Sci. B: Polym. Phys. 36, 983–989.
Sudarshan, K., Rath, S.K., Patri, M., Sachdeva, A., Pujari, P.K., 2007. Positron annihilation spectroscopic studies of fluorinated ethylene propylene copolymer-*g*-polystyrene. Polymer 48, 6434–6438.
Tanaka, K., Katsube, M., Okamoto, K., Kita, H., Sueoka, O., Ito, Y., 1992. Correlation between positron annihilation and gas diffusion properties of a series of polyimides. Bull. Chem. Soc. Jpn. 65, 1891–1897.
Tanaka, K., Kawai, T., Kita, H., Okamoto, K., Ito, Y., 2000. Correlation between gas diffusion coefficient and positron annihilation lifetime in polymers with rigid polymer chains. Macromolecules 33, 5513–5517.
Tao, S.J., 1972. Positronium annihilation in molecular substances. J. Chem. Phys. 56, 5499–5510.
Vie, P., Paronen, M., Strømgard, M., Rauhala, E., Sundholm, F., 2002. Fuel cell performance of proton irradiated and subsequently sulfonated poly(vinyl fluoride) membranes. J. Membr. Sci. 204, 295–301.
Wang, H., Capuano, G.A., 1998. Behavior of raipore radiation-grafted polymer membranes in $H_2/O_2$ fuel cells. J. Electrochem. Soc. 145, 780–784.
Yamaki, T., Kobayashi, K., Asano, M., Kubota, H., Yoshida, M., 2004. Preparation of proton exchange membranes based on crosslinked polytetrafluoroethylene for fuel cell applications. Polymer 45, 6569–6573.